Biosensors and Bioelectronics 25 (2009) 173–178

Contents lists available at ScienceDirect

Biosensors and Bioelectronics

journal homepage: www.elsevier.com/locate/bios

Toward real-time continuous brain glucose and oxygen monitoring with a smart catheter

Chunyan Li[a,b,*], Chong H. Ahn[b], Lori A. Shutter[a], Raj K. Narayan[a]

[a] Department of Neurosurgery, University of Cincinnati, Cincinnati, OH 45267, USA
[b] Department of Electrical and Computer Engineering, University of Cincinnati, Cincinnati, OH 45221, USA

ARTICLE INFO

Article history:
Received 20 April 2009
Received in revised form 21 June 2009
Accepted 22 June 2009
Available online 26 June 2009

Keywords:
Glucose sensor
Oxygen sensor
Traumatic brain injury
Lab-on-a-tube
Continuous monitoring

ABSTRACT

Oxygen and glucose biosensors have been designed, fabricated, characterized and optimized for real-time continuous monitoring on a new smart catheter for use in patients with traumatic brain injury (TBI). Oxygen sensors with three-electrode configuration were designed to achieve zero net oxygen consumption. Glucose sensors were based on the use of platinum nanoparticle-enhanced electrodes that were modified with polycation and glucose oxidase immobilized by chitosan matrix. An iridium oxide electrode was developed to work as a biocompatible reference electrode with enhanced durability and stability in the biological solutions. A study of the effect of temperature on oxygen sensor performance, and both temperature and oxygen effects on glucose sensor performance were accomplished to enhance their operative stability and provide useful information for *in vivo* applications. A new methodology for automatic correction of the temperature and oxygen dependence of biosensor outputs is demonstrated through programmed LabView™ software. *In vitro* experiments in both physiological and pathophysiological ranges (oxygen: 0–60 mmHg; glucose: 0.1–10 mM; temperature: 25–40 °C) with clinical samples of cerebrospinal fluid obtained from TBI patients have demonstrated stable measurements with enhanced accuracy, indicating the feasibility of the sensors for a real-time continuous *in vivo* monitoring.

Published by Elsevier B.V.

1. Introduction

Traumatic brain injury (TBI) disrupts the normal function of the brain and is a leading cause of morbidity and mortality worldwide. The pathophysiology of TBI is usually classified as primary and secondary events. Primary events include initial injury and variable degrees of irreversible neuronal damage or death. The secondary events involve a cascade of molecular, cellular and tissue processes in response to the initial injury, and therefore represent feasible targets of therapeutic interventions. The aim of TBI management in neuro-intensive care units (NICUs) is to prevent, detect and treat secondary brain injury in order to reduce injury progression and improve outcome. Recent clinical trials indicate that the multimodality approach to cerebral monitoring can improve patient outcome after TBI (Tisdall and Smith, 2007; Wartenberg et al., 2007; Wright, 2007; Kim, 2006; De Georgia and Deogaonkar, 2005; Mulvey et al., 2004).

The cellular damage that occurs after TBI is reflected in changes of cerebral metabolism and energy state in brain extracellular fluid (ECF) (Werner and Engelhard, 2007; Smith, 2005). Biochemical changes in ECF are early markers of the brain ischemia and hypoxia, which are central causes of brain damage in TBI patients (Belli et al., 2008; Tisdall and Smith, 2006). Thus, measurement of brain tissue biochemistry has the potential to provide early detection of secondary injury after TBI and guide therapy before further neuronal damage occurs. Neuronal survival relies on an adequate supply of oxygen and glucose from neighboring capillaries to generate adenosine triphosphate (ATP) by cerebral blood flow. Any decrease in perfusion in the brain causes additional secondary ischemia and injury, and thus may contribute to poor outcomes (Meixensberger et al., 1997). Previous studies have suggested that reduced ECF glucose concentration and tissue hypoxia are associated with poor outcomes after head injury (Schlenk et al., 2008; Vespa et al., 2003; Nortje and Gupta, 2006; Stevens, 2004). Since oxygen and glucose are critical for the recovery of injured tissue (De Georgia and Deogaonkar, 2005), simultaneously monitoring brain oxygen and glucose can be helpful for the early detection of secondary injury, and may enable prompt therapy.

Currently, two main devices, Licox (Integra Neuroscience) and Neurotrend (Codman), are used to measure brain tissue oxygen tension ($P_{bt}O_2$). Jugular bulb oximetry ($S_{jv}O_2$) is used in a very few centers to measure global cerebral oxygenation. Cerebral microdialysis (MD), which provides on-line brain tissue biochemistry, is also used by a very few investigators to measure ECF glucose concentrations. The disadvantages of the current $P_{bt}O_2$ and MD monitoring

* Corresponding author at: Department of Neurosurgery, University of Cincinnati, Cincinnati, OH 45267, USA. Tel.: +1 513 556 0903; fax: +1 513 556 7326.
E-mail address: lic2@ucmail.uc.edu (C. Li).

0956-5663/$ – see front matter. Published by Elsevier B.V.
doi:10.1016/j.bios.2009.06.032

techniques are that they only provide measurements for a small region of the brain, with wide variability throughout the injured brain tissue. Conversely, $S_{jv}O_2$ provides a measure of global cerebral oximetry, but is notoriously labor-intensive and tends to produce unreliable data and artifacts.

CSF oxygen partial pressure ($P_{csf}O_2$) has been proposed as a surrogate marker for brain tissue oxygenation and it is linearly related to the mean arterial oxygen pressure of brain tissues surrounding fluid spaces (Jankowska and Grieb, 1979; Anzai et al., 2004; Zaharchuk et al., 2005). In addition, glucose levels in the ECF are between 20% and 30%, and CSF glucose values are typically 50–70% of plasma glucose levels (Evans et al., 2003). Based on these relationships, simultaneous measurements of both ECF and CSF neurochemistry may make it possible to obtain a better understanding of the pathophysiology of secondary brain damage. We have previously developed a novel lab-on-a-tube (LOT), or smart catheter, which is capable of continuously monitoring multiple physiological and metabolic parameters, as well as draining CSF (Li et al., 2009). *In vitro* experiments with clinical samples of CSF obtained from TBI patients have demonstrated stable pressure, temperature, oxygen and glucose measurements for 5 days of continuous monitoring. By integrating microsensors both inside and outside the tube, it can simultaneously measure parameters both in ECF and CSF. In the present work, enhanced accuracy of oxygen and glucose microsensors for *in vivo* application were described with clinical samples from TBI patients. A biocompatible iridium oxide electrode was developed to work as a reference electrode in the three-electrode system to achieve minimal long-term drift of electrode potential in the biological solutions. Errors related to the temperature dependence for oxygen sensor outputs and both temperature and oxygen dependence for glucose sensor outputs were greatly reduced through programmed LabView™ software.

2. Design and working principle

Oxygen and glucose sensors were designed for long-term *in vivo* monitoring, while solving the associated major challenges (Wang, 2008a,b; Koschwanez and Reichert, 2007). For the operation of amperometric biosensors, it is desirable to isolate the reference electrode (RE) from participation in the electrochemical reaction (Bott, 1995). A Clark cell with three-electrode configuration can meet this demand and is employed for the development of oxygen and glucose sensors.

2.1. Reference electrode

The reference electrode is a key component of the electrochemical biosensor. To date, miniature Ag/AgCl electrodes have been used as a reference electrode for most applications. However, AgCl is toxic and the quantity of AgCl in microfabricated Ag/AgCl electrodes is very small. Moreover, AgCl is susceptible to reactions with electroactive species. One promising alternate material is iridium oxide (IrOx), which is biocompatible, mechanically stable and exhibits minimal long-term drift of electrode potential in fixed pH solutions (Ges et al., 2005; Yang et al., 2004a,b).

2.2. Oxygen sensor

In the three-electrode mode of operation, oxygen is reduced to hydroxyl ions at the working electrode (WE) and the hydroxyl ions are oxidized to oxygen at the counter electrode (CE) for alkaline solution (Yeager, 1984) as follows:

Electrochemical reaction at WE : $O_2 + H_2O + 4e^- \rightarrow 4OH^-$

Electrochemical reaction at CE : $4OH^- \rightarrow O_2 + 2H_2O + 4e^-$

In principle, there is no net consumption of oxygen nor production of hydroxyl ions (Karagounis et al., 1986). Solid polymer electrolyte (nafion) based oxygen sensors do not have the problems associated with liquid electrolyte dehydration, and they also provide protection against fouling.

2.3. Glucose sensor

For implantation applications, amperometric enzyme-based biosensors are currently superior to other sensor types due to the high selectivity of enzymes. The two representative enzymes are glucose oxidase (GOD) and pyrroloquinoline quinone glucose dehydrogenase (PQQ-GDH). GDH based amperometric glucose biosensors have the benefits of oxygen-independence and higher catalytic efficiency compared to GOD (Laurinavicius et al., 1999; Lau et al., 2007). However it suffers from either low substrate specificity or limited stability. On the other hand, GOD exhibits superior substrate specificity and enhanced operating stability; and hence is used in this work. Most *in vivo* glucose sensors rely on mediatorless-based detection of hydrogen peroxide due to potential leaching and toxicity of the mediator. Glucose is enzymatically converted to hydrogen peroxide (H_2O_2) by glucose oxidase, and the H_2O_2 that is so produced is electrochemically detected by the electrodes as summarized below (Miyashita et al., 2009):

Enzymatic reaction : $\text{Glucose} + O_2 \rightarrow \text{gluconolactone} + H_2O_2$

Electrochemical reaction at WE : $H_2O_2 \rightarrow 2H^+ + O_2 + 2e^-$

Electrochemical reaction at CE : $2H^+ + 1/2O_2 + 2e^- \rightarrow H_2O$

Platinum nanoparticles were electrochemically deposited on Au electrodes to provide a large available surface and enhance the electrocatalytic activity for the H_2O_2 for glucose sensor (Li and Lin, 2007; Luo et al., 2006). The polycation poly(allylamine) (PAA) is used to effectively eliminate interference (Yang et al., 2004a,b). Chitosan, which has good biocompatibility, chemical inertness, high mechanical strength and stable microenvironment around the enzyme, is used as a GOD matrix (Kang et al., 2008; Krajewska, 2004).

2.4. Automatic correction approach

Clark-type amperometric sensors are influenced by temperature, and this can result in a change of output readings. Hence, oxygen and glucose sensors need to be checked for their specific temperature sensitivity. In combination with a temperature sensor that continuously monitors environmental temperature, automatic correction for changes in temperature are programmed through LabView™ by the following equation:

$$I_{CT} = I_t + (I_t \times F_T)(T_{25} - T_t)$$

where I_{CT} is the calibrated current for temperature dependency of oxygen and glucose sensors (nA), T_t is the measured temperature at the time t by temperature sensor (°C), F_T is the temperature factor system (%/°C), and I_t is the current measured at the time t during experiments (nA).

Mediatorless-based glucose biosensors are also oxygen dependent, and therefore oxygen dependence of glucose sensors outputs are checked. Whenever oxygen tension decreases to less than 151 mmHg (air saturated), automatic correction for changes in oxygen tension are programmed through LabView™ by the following equation:

$$I_{CO} = \frac{I_{tT} \times S_{O151} - I_B}{S_{Ot}} + I_B$$

where I_{CO} is the calibrated current for oxygen dependency of glucose sensors (nA), I_{tT} is the current recorded at the time t after correction for temperature dependency (nA), I_B is the background current (nA), S_{O151} is the glucose sensitivity at the oxygen tension of 151 mmHg (nA/mM), and S_{Ot} is the glucose sensitivity at the oxygen tension of measured by oxygen sensor at the time t (nA/mM).

3. Experimental

3.1. Materials

Glucose oxidase (GOD) (EC 1.1.3.4, Type X-S, *Aspergillus niger*, 136,100 U/g), β-D-glucose, chitosan (MW ~ 10^5, 75–85% deacetylation), PAA solution, potassium platinum chloride (K_2PtCl_6), acetaminophen (AP), ascorbic acid (AA), uric acid (UA), glutaraldehyde (GA, 25%), Nafion® 117 (5%, w/w), acetic acid, sodium phosphate dibasic (Na_2HPO_4), and phosphate buffered saline (pH 7.4) were purchased from Sigma–Aldrich–Fluka. Iridium pellets (4N) were purchased from ESPI Metals (USA) and used as the metal source of the e-beam evaporator. RTV Silicone was obtained from M.G. Chemicals (USA). All chemicals were of analytical reagent grade and were used as received. Five calibration gases containing 1%, 2%, 3%, 5% and 8% oxygen concentrations were obtained from Wright Bothers Inc. (Cincinnati, USA). Human CSF that was drained from TBI patients in the course of their treatment, and was normally discarded was obtained from University Hospital, Cincinnati.

3.2. Apparatus

The model 215 benchtop research-grade pH/mV meter (Denver Instrument Corp., CO, USA) was used to measure the open circuit potentials (OCP) of iridium oxide (IrOx) relative to the Ag/AgCl (3 M NaCl). The dissolved oxygen content of the solution was measured with a dissolved oxygen meter (Oakton® DO 110, Fisher Scientific, USA). A FreeStyle™ blood glucose meter (Therasense, USA) was used for testing CSF glucose during experiments. A potentiostat (PalmSens, Palm Instruments BV, the Netherlands) provided all electrochemical functions necessary for the anodic oxidation of iridium and electroplating of platinum nanoparticles. A customized detection circuit built on the printed circuit board (PCB) with LabView™ control software was used to simultaneously measure glucose, oxygen and temperature outputs. Experiments were carried out in a temperature controlled waterbath (H-1390, Humboldt Mfg. Co., USA).

3.3. Device fabrication

Standard microfabrication processes were used for the development of oxygen, glucose and temperature microsensors. Briefly, a Kapton film (Dupont 100HN) was cleaned and attached to the 6 in. silicon wafer, which had been spin-coated with polydimethylsiloxane (PDMS, Sylgard 184A and 184B). Ti/Ir/Au (150 Å/500 Å/900 Å) layers were deposited using e-beam metal evaporator (Temescal FC1800, BOC Edwards Temescal, USA) and patterned. 3 μm thick Parylene layer was deposited using Parylene deposition system (Model PDS 2010 Labcoter 2, USA) and patterned using RIE (March CS1701 RIE, USA) with patterned AZ4620 thick photoresist as an oxygen plasma protection layer. Subsequently, the substrate was cleaned with acetone, methanol and DI water.

3.3.1. Iridium oxide reference electrode

The Au layer on the reference electrode was selectively etched by Au etchant (TFA). A three-electrode electrochemical setup was used with the Ir microelectrode as the working electrode, a Ag/AgCl electrode as the reference electrode (3 M NaCl), and a platinum foil

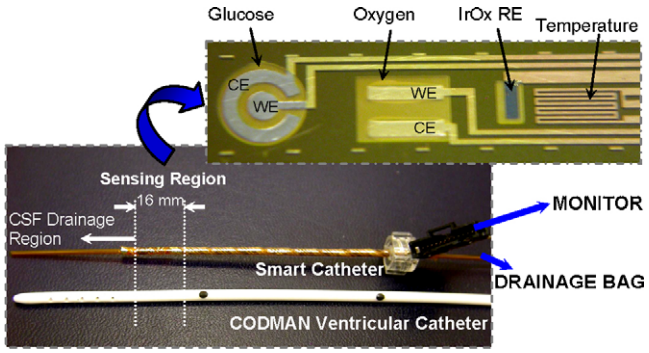

Fig. 1. Photographs of a smart catheter with glucose, oxygen and temperature sensors. Glucose sensor construction: Ti–Ir–Au/Pt nanoparticles/polycation/GOx/nafion; oxygen sensor construction: Ti–Ir–Au/nafion/silicone; reference electrode: Ti/Ir/IrOx/nafion; temperature sensor construction: Ti–Ir/Au/parylene.

(+99.99%) as the counter electrode. All electrodes were placed in an electrolyte solution of 0.7 M Na_2HPO_4. The IrOx layer was formed from Ir by employing repetitive potential pulses between −0.85 V and 0.75 V versus Ag/AgCl at a frequency of 0.5 Hz. Then, 0.5–1 μl nafion solution was applied on IrOx microelectrodes and annealed at 120 °C for 1 h.

3.3.2. Oxygen microsensor

1–1.5 μl nafion solution was applied on the oxygen working and counter electrodes as the polymer electrolyte membrane and dried at room temperature for 15 min. Subsequently, they were cured at 120 °C for 1 h. Finally, 1.5–2 μl RTV silicone solution was applied as the gas-permeable membrane and fully cured at room temperature for 8 h.

3.3.3. Glucose microsensor

A 1.0 wt.% chitosan solution was prepared by dissolving 1.0 g of chitosan in 100 ml of 1.0% acetic acid. The solution was stirred at 300 rpm for 3 h and cooled to room temperature. 0.5 mg PAA was dissolved in 0.5 ml of chitosan solution (1%), and then 10 μl of glutaraldehyde solution (2.5%) was added into the PAA-chitosan solution. 1 mg of GOD was dissolved in 0.5 ml of chitosan solution (1%), and then 10 μl of glutaraldehyde solution (2.5%) was added into the GOD-chitosan solution.

Platinum nanoparticles were electrochemically deposited by cyclic voltammetry in 0.5 M H_2SO_4 solution containing 2 mM K_2PtCl_6 by cycling 20 times between 0.4 V and −0.25 V at 50 mV/s. Then, 0.2–0.5 μl of PAA-chitosan solution was applied on the electrodes as the interference-free membrane and dried 2 h at room temperature. Subsequently, 2–3 μl of GOD-chitosan solution was applied and cured at room temperature for 4 h. Finally, 1.5–2 μl of nafion solution (5%) was applied as the outer membrane and cured at room temperature for 8 h.

3.3.4. Spirally rolling to form an intraventricular catheter

The Kapton film with temperature, oxygen and glucose microsensors were cut into size (width = 3.5 mm; length = 150 mm) and spirally rolled over the metal rod (CGSX-01, Small Parts Inc., USA) based on our previous work to form an intraventricular catheter (Li et al., 2008). Smart catheters were ready to use after they were soaked in a 2 mM glucose/PBS solution (pH 7.4) for 2 days.

Photographs of the fabricated device are shown in Fig. 1, which illustrate the gold RTD, oxygen microsensor and glucose microsensor. The entire smart catheter has an inner diameter (ID) of 1.5 mm, an outer diameter (OD) of 1.7 mm and a length of 110 mm. The length of the sensing region for the smart catheter is 16 mm.

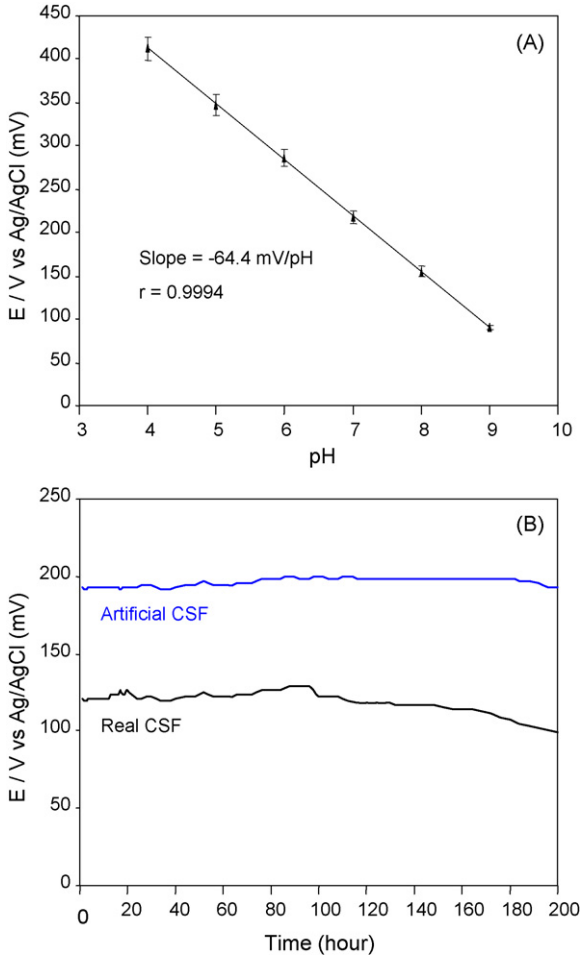

Fig. 2. Characteristics of IrOx reference electrodes: (A) pH dependence of IrOx OCP. (B) OCP change of IrOx electrodes in artificial CSF and real human CSF solutions.

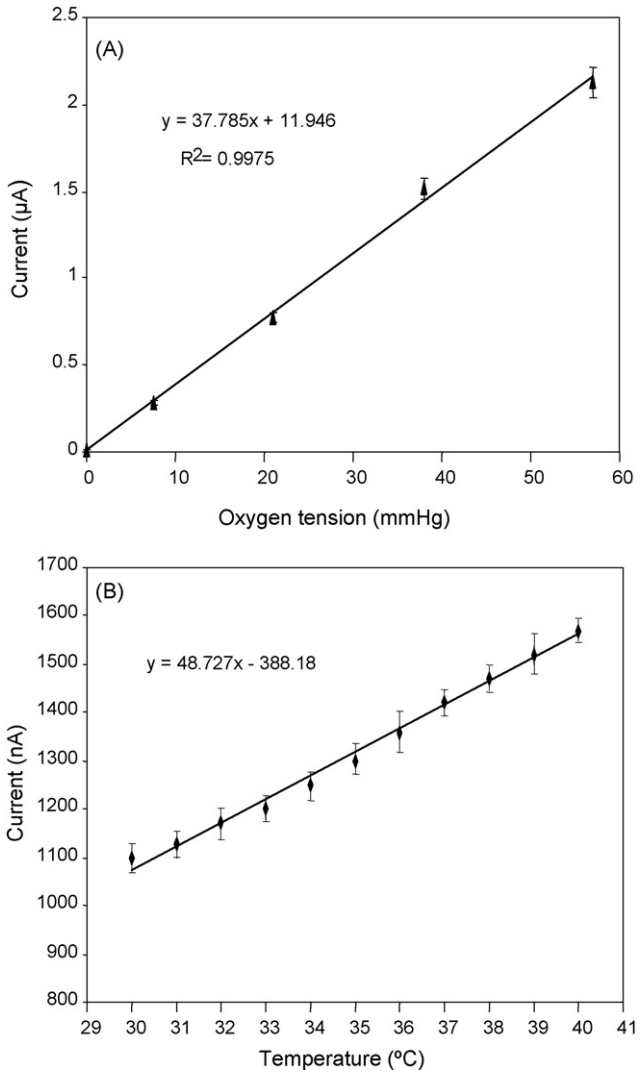

Fig. 3. Characteristics of oxygen microsensor: (A) calibration plot of the oxygen sensor in typical brain tissue oxygen tension range. (B) The effect of temperature on the oxygen sensor responses.

4. Results and discussion

Smart catheters were placed into a closed container filled with human CSF. The solutions were kept in a temperature controlled waterbath and equilibrated with calibration gases containing different oxygen concentration. The solutions were renewed every 8 h throughout the complete calibration and monitoring time.

4.1. Iridium oxide reference electrode

Coating the IrOx electrodes with nafion improved the stability and protected the electrodes from protein-promoted corrosion in aggressive biological solutions. A typical open circuit potential (OCP) response of the developed IrOx electrodes to pH changes was shown in Fig. 2(A). The results demonstrated a linear super-Nernstian response with a sensitivity of −64.4 mV/pH from pH 4 to pH 9 at 37 °C. Fig. 2(B) shows that the OCP drifts of IrOx electrodes are less than 29.8 mV in blood-stained CSF for 10 days. In general, brain pH is in the region of 7.15–7.4. Clinical evidence of brain stem death occurred when the pH approached about 7.05. Given such small dyanmic change of brain pH and that the pH dependence of the developed IrOx electrode potential is −64.4 mV/pH, the variance in IrOx electrode potential (less than ±50 mV) is negligible to introduce significant errors for amperometric biosensors that have wide diffusion dominant region (bigger than 100 mV for both oxygen and glucose sensors). Thus IrOx electrode is viable for continuous brain biosensors as a reference electrode. Because the concentration of CO_2 in CSF solution decreases due to the open state, the final pH of CSF solutions from five TBI patients used for the measurements were in the range of 8.4–8.9 with resulting average open circuit potential of 90 mV vs. Ag/AgCl RE. The potential of the working electrodes were maintained at 0.5 V and −0.7 V with respect to the IrOx RE respectively for glucose and oxygen sensors.

4.2. Oxygen microsensor

Normal $P_{bt}O_2$ values are in the region of 25–45 mmHg. A value below 15 mmHg is indicative of cerebral hypoxia that could lead to permanent neuronal injury. Oxygen sensors that can measure between 0 mmHg and 60 mmHg should account for all physiological ranges in the brain. *In vitro* calibration was carried out in CSF solutions that had been equilibrated at 37 °C with specified gas mixtures containing 1–8% oxygen. Fig. 3(A) shows the calibration curve for oxygen sensors. Good linearity with a correlation coefficient of 0.9975 and sensitivity of 37.785 nA/mmHg were observed. Clark-type oxygen sensors are influenced by temperature with a change of output readings. The effect of temperature on the responses of oxygen sensors was shown in Fig. 3(B). The temperature sensitivity of oxygen sensor is 48.7 nA/°C, which is approximately 3.5%/°C.

Table 1
Glucose content determination in CSF samples from TBI patients.

Sample number	From FreeStyle™ glucose meter (mM)	From fabricated glucose sensor (mM)
1	1.1	1.07 ± 0.01 (n = 4)
2	3.8	3.94 ± 0.03 (n = 5)
3	2.3	2.37 ± 0.01 (n = 6)
4	1.2	1.15 ± 0.01 (n = 4)
5	1.6	1.56 ± 0.02 (n = 5)

4.3. Glucose microsensor

Normal CSF glucose concentration ranges from 2.5 mM to 4.5 mM (Fishman, 2003). CSF glucose values are higher than in ECF with typical values being 50–70% of plasma glucose. As a result, glucose sensors that can measure between 0.1 mM and 10 mM should account for both normoglycemic and hypo- and hyperglycemic ranges in brain (ECF and CSF). A FreeStyle™ blood glucose meter was used for testing glucose concentration in human CSF samples. Glucose concentration in CSF samples was then adjusted by glucose solution prepared with artificial CSF. Fig. 4(A) illustrates the calibration curve for the glucose sensors at the tempertaure of 37 °C and pO_2 of 38 mmHg. They have the sensitivity of 67.366 nA/mM in the linear range from 0.1 to 10 mM with the linear coefficient of R^2 = 0.9995. Fresh CSF samples were first analyzed using FreeStyle™ blood glucose meter. The samples were then reassayed with developed glucose sensors. The results were shown in Table 1. As can be seen, the results were satisfactory and agree closely with those measured by the commercial glucose meter.

Temperature is an important factor for the overall kinetics of the glucose biosensors with enzyme reactivity increasing with temperature (Suelter, 1990). Fig. 4(B) shows the effect of temperature on the current response of the glucose microsensors. The output current at certain concentration increased with temperature until 40 °C with temperature sensitivity of 8.56 nA/°C. GOD based biosensors rely on the use of oxygen as the physiological electron acceptor, so oxygen supply can influence sensor output. Fig. 4(C) shows the calibration curve of glucose sensors measured under different oxygen tensions. Glucose sensors maintain more than 82% of their response to 10 mM glucose when the oxygen tension was over 58 mmHg. When the oxygen tension decreased to 23 mmHg, about 53% of the response was retained and the response of glucose was not satisfactorily linear. Electroactive species such as AA, UA and AP can interfere with the detection of hydrogen peroxide produced by the enzymatic reaction. The PAA membrane results in excellent permselectivity for the complete sensors. The effect of the interferents on the glucose sensor was investigated in the presence of their physiological levels with a glucose concentration of 2 mM. The ratio of I_{G+1} (response current to 2 mM glucose in presence of interferents) to I_G (response current to 2 mM glucose) was 1.021 for 0.1 mM AA, 1.013 for 0.5 mM UA, and 1.035 for 0.2 mM AP.

4.4. Auto correction using LabView™ program

Temperature dependence for the oxygen sensor, and both temperature and oxygen dependence for the glucose sensor were corrected through programmed LabView™ software. After automatic correction for temperature effect, the errors for oxygen sensors were reduced from 13.6 mmHg to 3.4 mmHg when the temperature was changed from 37 °C to 30 °C (Fig. 5(A)). As shown in Fig. 5 (B), after correction the errors were reduced from 1.4 mM to 0.6 mM for glucose sensor when the temperature was changed from 37 °C to 25 °C. The errors were also reduced from 4.3 mM to 0.4 mM when oxygen tension was changed from 151 mmHg to

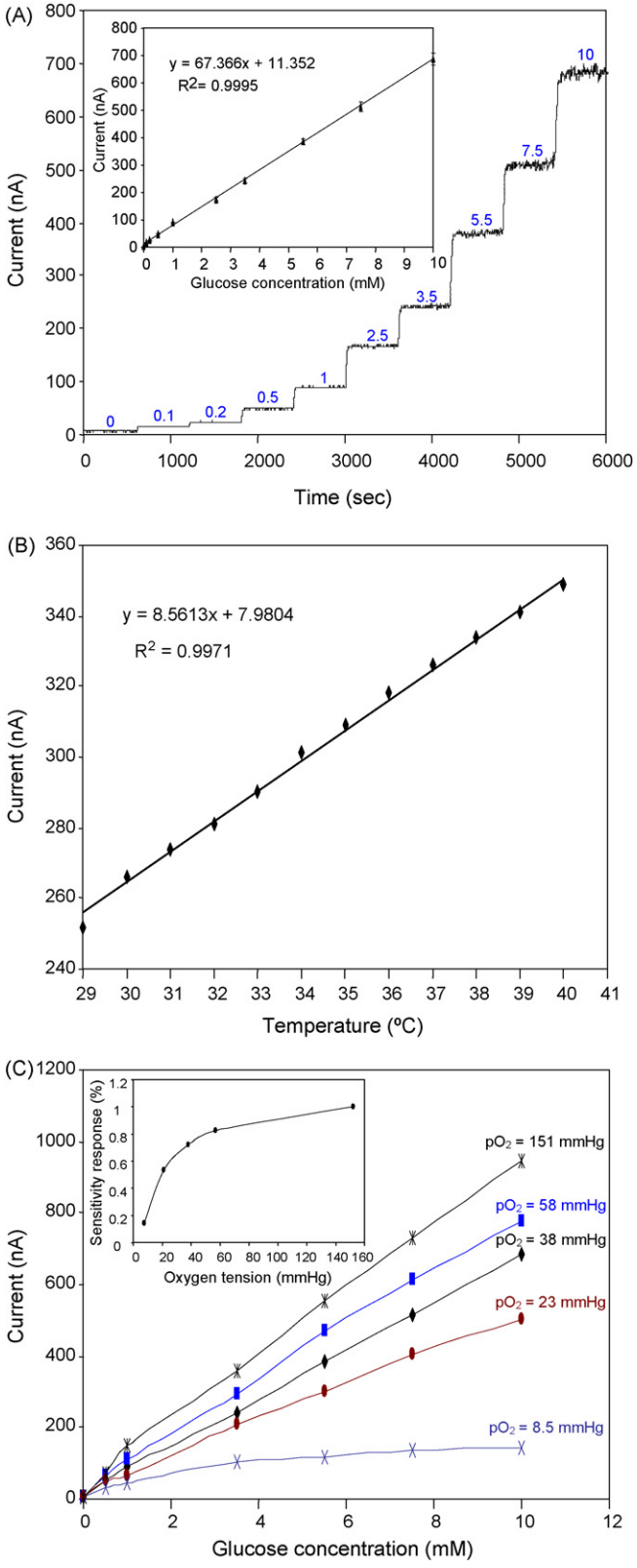

Fig. 4. Characteristics of glucose microsensor: (A) dynamic glucose response curve at pO_2 = 38 mmHg and T = 37 °C. (Inset) Calibration curve. (B) The effect of temperature on amperometric response current of the sensor. (C) *In vitro* oxygen effect on glucose sensors. (Inset) calibration plot for glucose sensor sensitivity response for different oxygen tension.

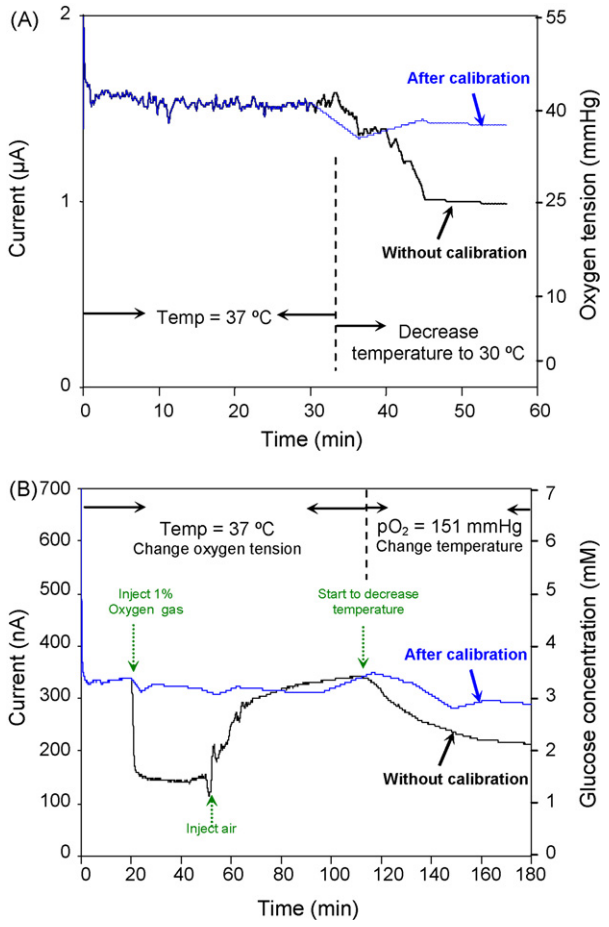

Fig. 5. Characteristics of auto-calibration using LabView™ program: (A) oxygen microsensor: pO_2 is 38 mmHg and temperature is changed from 37 °C to 30 °C. (B) Glucose microsensor: first temperature is kept at 37 °C and oxygen tension is changed from 151 mmHg to 8.3 mmHg; then pO_2 is kept at 151 mmHg and temperature is changed from 37 °C to 25 °C.

8.3 mmHg. Much greater improvement in accuracy may be achieved after calibration of both sensors under more detailed conditions in future.

5. Conclusion and outlook

Oxygen and glucose sensors on the new smart catheter have been designed, fabricated, and optimized to improve their accuracy and reliability by addressing some of the major challenges for *in vivo* biosensors. The metrological properties of the developed oxygen and glucose microsensors, as measured in the physiological and pathophysiological ranges *in vitro*, are satisfactory to continuously measure both parameters in human cerebrospinal fluid. The accuracy of oxygen and glucose sensors was greatly improved by using iridium oxide reference electrode and automatic correction for temperature and oxygen effect through external LabView™ software. The next step will be to conduct a trial of the smart catheter *in vivo* using an animal model. The use of the smart catheter for multimodal neuromonitoring of patients is in its infancy. However, the experimental results presented above suggest that it can transition from the research laboratory engineering benchtop into animal-based models in order to set the stage for clinical trials.

Acknowledgements

The work was supported by the Integra Lifesciences Foundation. The authors wish to thank Mr. Ron Flenniken of the Nano/Micro Fabrication Engineering Research Center at the University of Cincinnati for his technical support with the e-beam deposition of Iridium, and also Mr. Michael Rust at the Microsystems and BioMEMS lab for his valuable discussions.

References

Anzai, Y., Ishikawa, M., Shaw, D.W.W., Artru, A., Yarnykh, V., Maravilla, K.R., 2004. AJNR Am. J. Neuroradiol. 25, 274–279.
Belli, A., Sen, J., Petzold, A., Russo, S., Kitchen, N., Smith, M., 2008. Acta Neurochir. (Wien.) 150, 461–470.
Bott, A.W., 1995. Current Separations 14, 64–68.
De Georgia, M.A., Deogaonkar, A., 2005. Neurologist 11, 45–54.
Evans, M.L., Cherrington, A.D., Moore, M.C., Sherwin, R.S., 2003. In: Porte, D., Sherwin, R.S., Baron, A., Ellenberg, M., Rifkin, H. (Eds.), Ellenberg and Rifkin's Diabetes Mellitus: Theory and Practice. McGraw-Hill Professional, pp. 117–126.
Fishman, R.A., 2003. In: Warrel, D.A., Cox, T.M., Firth, J.D., Benz, E.J. (Eds.), Lumbar Puncture. Oxford University Press, New York, pp. 953–955.
Ges, I.A., Ivanov, B.L., Schaffer, D.K., Lima, E.A., Werdich, A.A., Baudenbacher, F.J., 2005. Biosens. Bioelectron. 21, 248–256.
Jankowska, L., Grieb, P., 1979. Am. J. Physiol. 236, F220–225.
Kang, X., Mai, Z., Zou, X., Cai, P., Mo, J., 2008. Talanta 74, 879–886.
Karagounis, V., Lun, L., Liu, C.C., 1986. IEEE Trans. Biomed. Eng. BME 33 (2), 108–112.
Kim, D.H., 2006. Neurocrit. Care 4, 83–92.
Koschwanez, H.E., Reichert, W.M., 2007. Biomaterials 28 (25), 3687–3703.
Krajewska, B., 2004. Enzyme Microb. Technol. 35, 126–139.
Lau, C., Borgmann, S., Maciejewska, M., Ngounou, B., Gründler, P., Schuhmann, W., 2007. Biosens. Bioelectron. 22, 3014–3020.
Laurinavicius, V., Kurtinaitiene, B., Liauksminas, V., Ramanavicius, A., Meskys, R., Rudomanskis, R., Skotheim, T., Boguslasky, L., 1999. Anal. Lett. 32, 299.
Li, C., Wu, P.M., Han, J., Ahn, C.H., 2008. Biomed. Microdevices 10, 671–679.
Li, C., Wu, P.M., Jung, W., Ahn, C.H., Shutter, L.A., Narayan, R.K., 2009. Lab Chip 9, 1988–1990.
Li, J., Lin, X., 2007. Biosens. Bioelectron. 22, 2898–2905.
Luo, X., Morrin, A., Killard, A.J., Smyth, M.R., 2006. Electroanalysis 18 (4), 319–326.
Meixensberger, J., Jager, A., Dings, J., Baunach, S., Roosen, K., 1997. In: Bauer, B.L., Kuhn, T.J. (Eds.), Severe Head Injuries. Springer Verlag, New York, NY, pp. 99–108.
Miyashita, M., Ito, N., Ikeda, S., Murayama, T., Oguma, K., Kimura, J., 2009. Biosens. Bioelectron. 24, 1336–1340.
Mulvey, J.M., Dorsch, N.W.C., Mudaliar, Y., Lang, E.W., 2004. Neurocrit. Care 1 (3), 391–402.
Nortje, J., Gupta, A.K., 2006. Br. J. Anaesth. 97 (1), 95–106.
Schlenk, F., Nagel, A., Graetz, D., 2008. Intensive Care Med. 34, 1200–1207.
Smith, M., 2005. Anaesthesia, Pain, Intensive Care and Emergency Medicine. A.P.I.C.E. Springer Milan Publisher, pp. 139–146.
Stevens, W.J., 2004. J. Neurosci. Nurs. 36 (6), 332–339.
Suelter, C.H., 1990. Experimentelle Enzymologie Grundlagen f˙ur die Laborpraxis. Gustav Fischer Verlag, Stuttgart.
Tisdall, M.M., Smith, M., 2006. Br. J. Anaesth. 97 (1), 18–25.
Tisdall, M.M., Smith, M., 2007. Br. J. Anaesth. 99 (1), 61–67.
Vespa, P.M., McArthur, D., O'Phelan, K., et al., 2003. J. Cereb. Blood Flow Metab. 23, 865–877.
Wang, J., 2008a. Chem. Rev. 108 (2), 814–825.
Wang, J., 2008b. Talanta 75, 636–641.
Wartenberg, K.E., Schmidt, J.M., Mayer, S.A., 2007. Crit. Care Clin. 23, 507–538.
Werner, C., Engelhard, K., 2007. Br. J. Anaesth. 99 (1), 4–9.
Wright, W.L., 2007. J. Neurol. Sci. 261, 10–15.
Yang, H., Kang, S.K., Choi, C.A., Kim, H., Shin, D.H., Kim, Y.S., Kim, Y.T., 2004a. Lab Chip 4, 42–46.
Yang, M., Yang, Y., Liu, B., Shen, G., Yu, R., 2004b. Sens. Actuators B 101, 269–276.
Yeager, E., 1984. Electrochim. Acta 29, 1527–1537.
Zaharchuk, G., Martin, A.J., Rosenthal, G., Manley, G.T., Dillon, W.P., 2005. Magn. Reson. Med. 54, 113–121.